Metal−Metal Coordination Chemistry: Free Clusters of Group 11 Elements with Sodium[§]

Ueli Heiz,*,[†,‡] Arthur Vayloyan,[‡] and Ernst Schumacher[‡]

Institut de Physique Expérimentale, Université de Lausanne, CH-1015 Lausanne, Switzerland, and Institute for Inorganic and Physical Chemistry, University of Bern, CH-3000 Bern 9, Switzerland

Received: March 28, 1996; In Final Form: June 10, 1996[⊗]

Mixed metal clusters of sodium with copper, silver, and gold were produced by supersonic expansions at well-defined thermodynamic conditions. Differences in the behavior toward binary alloying, cluster formation, and relative thermodynamic stabilities are discussed within a structureless, delocalized, electronic shell model and using molecular orbital arguments and the different strengths of the relativistic effects of the coinage metals. Free-energy changes (ΔG) of selected exchange reactions are determined, showing the substitution of gold atoms to be thermodynamically the most favored. This is due to the preferred s−d hybridization in gold atoms, leading to a stronger metal−metal interaction. The measured ionization potentials reveal a distinct shell closing at the octamer for all three heterosystems. The drop of the ionization potential going from the octamer to the nonamer is most pronounced for the sodium−silver heteroclusters and is almost as large as for pure sodium clusters.

1. Introduction

Alloys and particularly binary alloys have received special attention in recent years due to their unique physical and chemical properties.[1] Advances in metallurgy have resulted in a whole variety of different alloys with almost customized properties, ranging from metallic to semiconducting ones.[2−4] Today these materials are indispensable in fields such as electrochemistry, catalysis, microelectronics, magnetooptics, and structural material science. In all these cases, an understanding of the heteronuclear metal−metal bond is crucial in order to design and master new bimetallic materials. In the age of nanotechnology, heterometallic materials with sizes beginning at only a couple of atoms are becoming relevant and an understanding of the development of the heterometallic bond going from such small assemblies to solid−state alloys is of fundamental interest. However, a coherent description of these bimetallic bonds in systems as diverse as solids, surface alloys, and heteroclusters is far from complete.

In solids, the strength of the bimetallic bond determines the structure of the alloy. Alloys showing an ordered structure can be treated with simple models, as the translational symmetry of the Bravais lattice in these systems allows them to be described with the ansatz of Bloch. In disordered alloys, the consequences are more drastic, as the assignment of the atoms to sites is random and Bloch's theorem breaks down. Typical phenomena of disordered alloys such as the unusual temperature dependence of the resistance are explained by treating the alloy by an impurity model.[5−7] The characterization of the bimetallic bonding at surfaces is even more complex. Besides alloying, surface enrichment of a certain element may be observed if its metal−metal bond is weak. If one of the elements has a larger radius, it may also segregate into the bulk due to strain energy. In both cases, the term surface alloy becomes obsolete. However, the consequences of surface alloying or adlayer formation are important, since the reduction in the atomic coordination at the surface produces a narrowing of the valence band. To maintain a common Fermi level, electrons have to flow between the surface and the bulk of the bimetallic system. This in turn changes the character of the metal−metal bond at the surface with respect to the bulk.[8,9]

The question arises as to whether these concepts of bimetallic bonds in solids and surfaces and their influence on their structure are also valid for clusters. In heteroclusters, the term alloy may become ambiguous. Do we consider a heterometallic dimer or a cluster consisting of a central atom and a finite metal ligand sphere as an alloy? How do we define migration or miscibility in a cluster of the size of a couple of atoms, and what do we understand by ordered and disordered heteroclusters? To what extent is the geometrical structure or the electronic structure relevant to heterocluster stabilities? Despite these questions, clusters are particularly important in that they are the link between atomic surface and bulk properties. Small clusters are surfacelike, and with increasing size, we observe a transition from surfacelike to bulklike clusters. These considerations underscore the need to learn more about the metal−metal bond in these small particles. In previous work, it was shown that small sodium heteroclusters with one atom of Cd/Zn/Hg are van der Waals molecules, whereas the same heteroclusters with more than six atoms are metal-bonded clusters.[10] Such a transition could not be found for Li/Na or Na/K heteroclusters, however.[11,12] Experiments on very small CsAu clusters suggest that the ionic character is already developed in this small size range.[13] In another set of experiments, the measurements of ionization potentials suggested that many bimetallic clusters behave like almost perfect jellium clusters,[14−17] e.g., structureless entities with more or less spherical shapes.

This work is a continuation of these studies of metal−metal coordination chemistry and investigates the interaction of sodium with the noble metals copper, silver, and gold, which have an ns^1 configuration with a $^2S_{1/2}$ ground state. In contrast to previous experiments, these heteroclusters were formed in a two-chamber oven under well-defined thermodynamic conditions. The cluster formation of these three types of systems was investigated, and the results are discussed using molecular orbital and geometrical arguments and relativistic effects, as well as jellium calculations. Due to the observation of binomial cluster distributions, enrichment factors of the heteroatom in the cluster could be determined. From these enrichment factors, the free energies of some selected elementary steps during cluster

§ 8th International Symposium on Small Particles and Inorganic Clusters ISSPIC 8. *Book of Abstracts*; Lindelof, P. E., Ed.; University of Copenhagen, Denmark, July 1−6, 1996.

* E-mail: Ulrich.Heiz@ipe.unil.ch. Fax: ++ 41 21 692 36 35.
† Université de Lausanne.
‡ University of Bern.

⊗ Abstract published in *Advance ACS Abstracts,* August 15, 1996.

S0022-3654(96)00938-0 CCC: $12.00

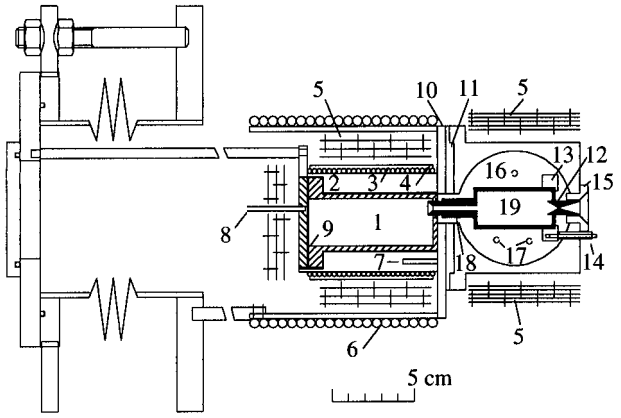

Figure 1. Two-chamber oven: large cartridge made of molybdenum (1), stainless steel cartridge holder (2), thermocoax heater (Philips ZEZ I 20) (3), cylindrical thermocoax holder (4), tantalum shielding (5), water-cooled stainless steel cylinder (6), Ni/Cr−Ni thermocouple (7, 8), graphite gasket (9), molybdenum plate (10), ceramic insulator (11), conical nozzle (12), graphite ring (13), Pt/Pt−Rh thermocouple (14), graphite cone (15), thermal mirror made of molybdenum (16), tungsten heating wires of diameter 0.7 mm and length 450 mm (17), connecting piece (18), high-temperature cartridge made of molybdenum (19).

formation were then calculated and compared with solid-state and dimer results. For selected heteroclusters, photoionization efficiency curves were measured, and from these, vertical ionization potentials were extracted.

2. Experimental Details

The experimental methods used for this work were the generation of mixed metal clusters, the measurement of heterocluster abundances with ionization mass spectrometry, and the determination of ionization potentials by measuring the photoionization efficiency (PIE) curves. The experiments were carried out in a supersonic molecular beam apparatus which is described in detail elsewhere.[18] Briefly, it consists of two differentially pumped vacuum chambers. The heteroclusters were generated in the first chamber by nonseeded expansions from a newly designed two-chamber oven, which is described below. This chamber was pumped with a 3000 L/s diffusion pump. The analysis chamber was pumped with a turbo molecular pump (500 L/s) and equipped with a quadrupole mass spectrometer (Extrel C50). This mass filter was mounted perpendicularly to the molecular beam and has an upper mass limit of 4000 amu. The mass-filtered ion current was amplified by a dynode/channeltron combination. Several viewports on the analysis chamber served as entrances for the ionizing photons supplied by an excimer pumped dye laser or an arc lamp. The radiation of the 1-kW Xe arc lamp, which has an unstructured emission spectrum below 380 nm, was dispersed through a 0.25-m monochromator (PTI; 1200 lines/mm, grating blazed at 300 nm). The photon flux was measured with a EMI 9783 B photomultiplier whose spectral response had been calibrated.

2.1. Two-Chamber Oven. A new cluster source was built for the generation of heteroclusters of alkali metals with alkaline-earth or transition metals. The basic idea was to design a supersonic nozzle two-chamber oven with the possibility of heating two different metals independently. In this way, the cluster formation of different heterosystems and cluster stabilities can be compared directly, as the partial pressures of the two metals can be set to well-defined values during the whole experiment. This results in constant and equal thermodynamic conditions during the supersonic expansion.

This new heterocluster source is shown in Figure 1. Basically it consists of two separately heatable cartridges made of molybdenum. The larger one (1) is heated with a thermocoax heater (3). It is protected against radiation losses with three layers of tantalum foil (5) and surrounded by a water-cooled stainless steel cylinder (6). Typically this part can be heated up to 1220 K. The temperature is measured with a Ni/CrNi thermocouple (7). A second smaller cartridge (19) is heated with three tungsten wires (17), each of 0.7-mm diameter and 450-mm length. The cartridge is surrounded by a polished spherical thermal mirror (16) made of molybdenum with an infrared reflectivity of more than 80%. The whole mirror is shielded with five tantalum foils (5). Temperatures up to 1800 K at a heating power of 2.6 kW can be obtained as measured with a Pt/Pt−Rh thermocouple (14). This small, high-temperature cartridge has a conical nozzle (12) with a diameter of 0.5 mm. The two cartridges are linked with a thin-walled tube (18) to minimize heat transfer. One end of this tube is welded to the large cartridge, whereas to the other end small, exchangeable cartridges for the high melting point metals can be screwed on. The two cartridges are insulated by a ceramic disk (11) in order to maintain a difference in temperature of 1000 K for at least 3 h.

2.2. Cluster Generation. For each coexpansion, the large cartridge was filled with 20 g of sodium and the high-temperature cartridge with about 2 g of copper, 4 g of silver, or 6 g of gold, respectively (all materials in p.a. purity). Before use, the oxide layer of the sodium was removed mechanically and the metal subsequently cleaned in hexane. Prior to use, the copper rods were cleaned in nitric acid and distilled water. The oxide layer of silver was removed by annealing. Gold needed no pretreatment.

Before heating the cluster source, the oven vacuum chamber was pumped to 3×10^{-6} Torr and the detection chamber to 5×10^{-7} Torr. During the heating procedure, it was important to keep the small cartridge hotter than the large one to prevent clogging of the nozzle.

The final temperature of the sodium-containing cartridge was 1100 K for all coexpansions. This corresponds to a sodium pressure of 453 Torr. For the first set of experiments, the final temperatures of the small cartridge were 1650 K for the coexpansion with copper, 1400 K for the one with silver, and 1800 K for gold. These temperatures correspond to a vapor pressure of 0.05 Torr. In the second set of experiments, the Na/Cu and Na/Ag systems were studied at a temperature of the small cartridge of 1800 K.

For each heterosystem, the relative sodium cotent in the cluster beam was measured as a function of time, evaluating the mass spectra taken every 10 min during the coexpansion. It turned out that 10 min after the first ion signal was detected, a stable molecular beam, e.g., a molecular beam with a constant sodium mole fraction and constant beam intensity, could be maintained for 80 min. This also defined the time frame of the experiments.

2.3. Neutral Cluster Abundances. The central problem in the interpretation of photoionization mass spectra is how to get neutral cluster abundances from the measured ion currents. The degree of the conversion of neutral clusters into ion current depends on (a) the detection efficiency of the experimental setup, (b) the relative ionization cross sections of the different clusters, and (c) the possible fragmentation processes during ionization. In order to diminish instrument-specific factors, the settings of the mass spectrometer and the position of the Xe arc lamp were always optimized to maximize the ion current for the largest detectable cluster in the beam. In this way, we compensate for the decreased detection efficiency in the higher mass range,[19] as it was shown that in our experimental setup, mass discrimina-

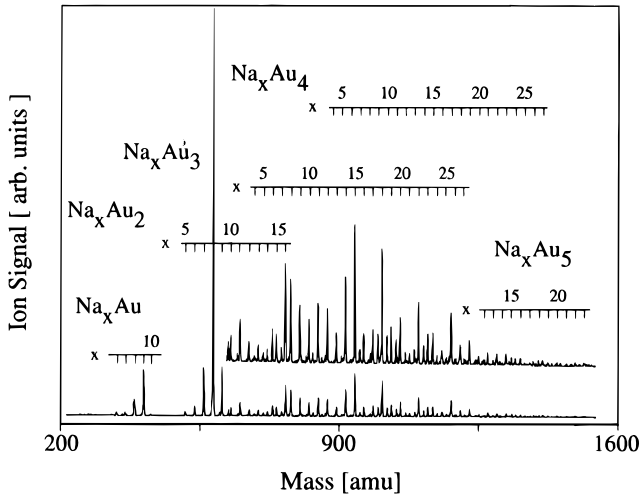

Figure 2. Representative photoionization mass spectrum for a Na/Au expansion, cluster beam ionized at 300 nm. Heterocluster distributions with one to five gold atoms are separately labeled. Outstanding are the predominance of Na_8Au_2 and the closed shells at the 10-atom cluster (Na_9Au, Na_8Au_2) and the 18-atom cluster ($Na_{16}Au_2$). Similar closed shells cannot be observed for heteroclusters with more than two gold atoms.

tion effects vary monotonically with cluster size.[11] Therefore, we equate relative ion currents with actual ion abundances. The most critical point is the conversion efficiency of the neutral clusters to their ions. This is mainly influenced by the different ionization cross sections of the individual clusters. To obtain the neutral cluster abundances, the photoionization mass spectra recorded with monochromator slits of 5 mm (16.5-nm fwhm (full width at half-maximum)) were corrected using relative differential ionization cross sections obtained from photoionization efficiency (PIE) curves.[10] These were measured with both 5-mm and 2-mm slits (6.6-nm fwhm). Five-millimeter-slit PIE measurements provided rough data for this correction, and from the 2-mm-slit measurements, ionization thresholds were extracted. Fragmentation of the heteroclusters occurs if enough excess energy is provided during the ionization process, leading to direct fragmentation or fragmentation by intermolecular vibrational energy redistribution. It has been shown that the energy threshold for significant fragmentation within the time scale of the experiment lies roughly 0.5 eV above the appearance potential.[20,21] From this, we conclude that our mass spectra taken at 300 nm are also free from fragmentation.

Due to these considerations we are confident that the neutral cluster abundances shown are not influenced by different ionization cross sections and fragmentation processes and are free from instrumental artifacts.

3. Results

3.1. Ionization Mass Spectra and Photoionization Efficiency (PIE) Curves of Mixed Heteroclusters. Figure 2 shows a typical photoionization mass spectrum obtained by irradiation with a Xe lamp through a 5-mm monochromator slit at 300 nm for a coexpansion of gaseous sodium and gold. The temperatures of the sodium and the gold cartridges were 1100 and 1800 K, respectively. The most striking feature is the predominance of the Na_8Au_2 species. Its intensity is 1−2 orders of magnitude greater than those of the other heteroclusters. The sodium/gold coexpansion also shows a good heterocluster formation. Clusters with up to five gold atoms were detected. Sharp relative maxima in cluster stabilities were observed for Na_9Au, $Na_{19}Au$ (not marked in Figure 2), Na_8Au_2, and $Na_{16}Au_2$. For the tri-, tetra-, and pentaheteroclusters, relative maxima

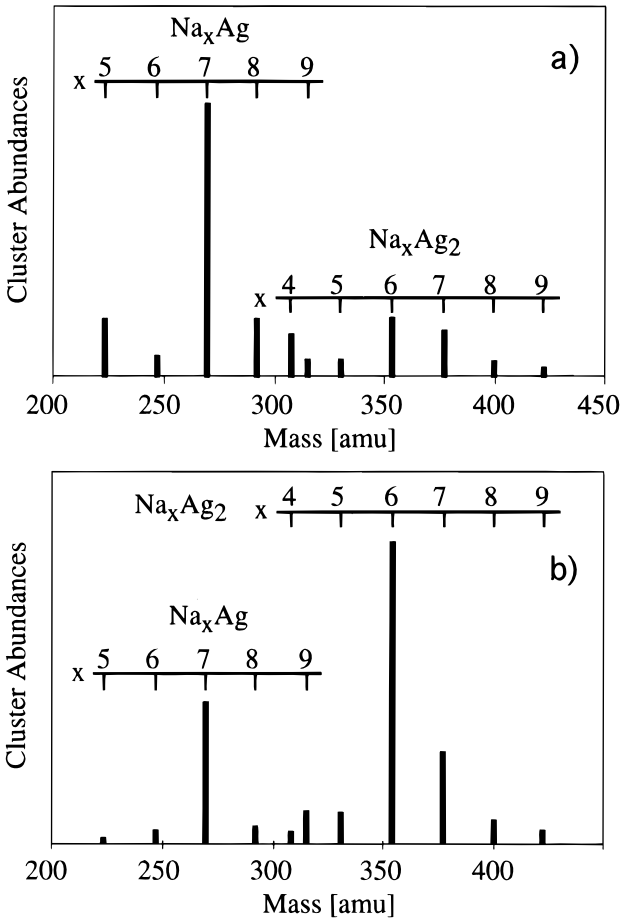

Figure 3. Neutral cluster abundances of two different Na/Ag expansions. The expansion temperatures were (a) 1100/1400 K and (b) 1100/1800 K. These data are extracted from photoionization mass spectra with an ionizing wavelength of 300 nm. Note the sharp abundance maxima at the eight-atom clusters Na_7Ag and Na_6Ag_2 in b are indicative of a thermodynamically controlled expansion.

are much less distinct and were observed for Na_8Au_3, $Na_{15}Au_3$, $Na_{18}Au_3$, and $Na_{22}Au_3$ for the triheteroclusters, Na_9Au_4, $Na_{10}Au_4$, $Na_{15}Au_4$, $Na_{17}Au_4$, $Na_{21}Au_4$, and $Na_{22}Au_4$ for the tetraheteroclusters, and finally $Na_{15}Au_5$, $Na_{16}Au_5$, $Na_{18}Au_5$, $Na_{22}Au_5$, and $Na_{23}Au_5$ for the pentaheteroclusters. For the mono-, di-, and triheteroclusters where the photoionization efficiency curves were measured, the resulting correction of the mass spectra did not result in a significant change of the sharp relative maxima. Therefore, the corrected mass spectra are not presented.

In Figures 3 and 4, the neutral cluster abundances obtained from the photoionization mass spectra of the systems Na/Ag and Na/Cu after normalization with the relative ionization cross sections are displayed. In these spectra, the expression $I_{ms(\lambda_i,z)}/I_{PIE(\lambda_i)}$ gives the corrected spectrum for every cluster z with I_{ms} being the measured intensity and λ_i the wavelength median of the window i. The mass spectra used to extract $I_{ms(\lambda_i,z)}$ were recorded at 300 nm.

The Na/Ag system demonstrates a fairly good cluster formation with the detection of heteroclusters with up to three silver atoms. The corresponding neutral cluster abundances are shown in Figure 3a. A distinct relative abundance maximum for Na_7Ag and a broad cluster distribution around the relative maximum at Na_6Ag_2 is observed for the mono- and diheteroclusters, respectively. This broad cluster distribution is typical for expansion conditions which are not yet fully thermodynamically controlled. In fact, at a higher small-cartridge temperature (1800 K), and thus higher internal cluster temperatures, a distinct

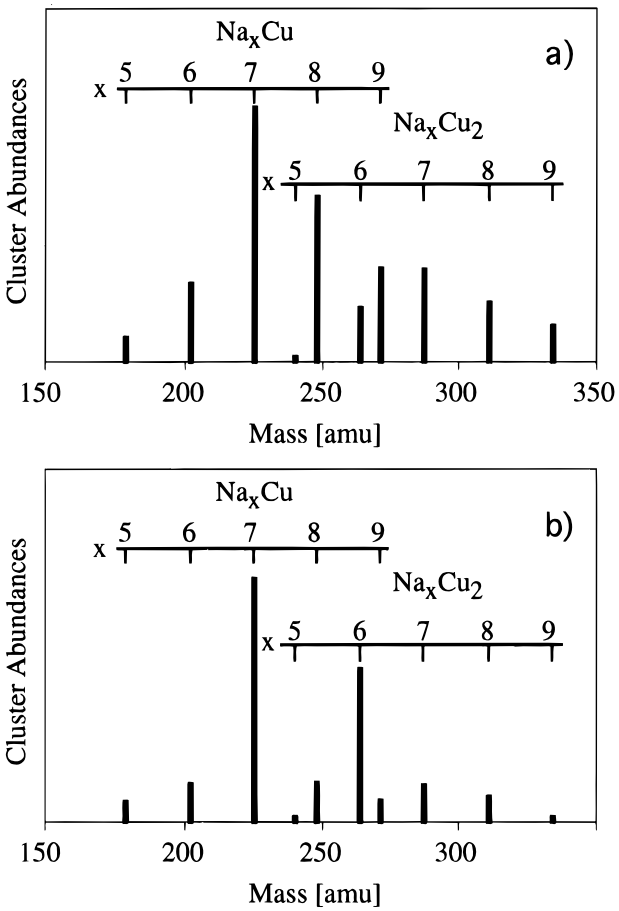

Figure 4. Neutral cluster abundances of two different Na/Cu expansions. The expansion temperatures were (a) 1100/1650 K and (b) 1100/1800 K. These data are extracted from photoionization mass spectra with an ionizing wavelength of 300 nm. Note the sharp abundance maxima at the eight-atom clusters Na_7Cu and Na_6Cu_2 in b.

relative maximum for Na_6Ag_2 occurs (Figure 3b). The same experiment also showed higher shell closings for $Na_{19}Ag$ and $Na_{18}Ag_2$ (not shown in Figure 3). The triheteroclusters revealed a corrected abundance maximum at Na_5Ag_3 and uncorrected relative maxima at $Na_{10}Ag_3$, $Na_{11}Ag_3$, and $Na_{17}Ag_3$, although these are much less pronounced.

The cluster formation for the Na/Cu system is the poorest of all three heterosystems, with cluster ion signals smaller by a factor of 20. The mono- and dicopper heteroclusters exhibit a broad cluster distribution around the relative maxima of Na_7Cu and Na_7Cu_2, respectively (Figure 4a). At higher expansion temperatures, sharp maxima for Na_7Cu and Na_6Cu_2 are observed (Figure 4b). Heteroclusters with a higher copper content were not detected.

Figures 5 and 6 show the photoionization efficiency (PIE) curves normalized for the photon flux of the heteroclusters Na_xY and Na_xY_2 ($x = 6-9$; Y: Cu, Ag, Au). As a comparison, the PIE curves of the pure sodium clusters are also included.[22] The monochromator slit used for all these measurements was 2 mm, which corresponds to 6.6-nm fwhm. The pseudo-Watanabe ionization potentials[19] from these PIE curves are summarized in Table 1.

4. Discussion

In the first part of this section, the results of the cluster abundance spectroscopy are discussed using a modified jellium model to compare the generated jellium numbers with the observed cluster stabilities. An interpretation of the different clustering of the three systems is found to be beyond this

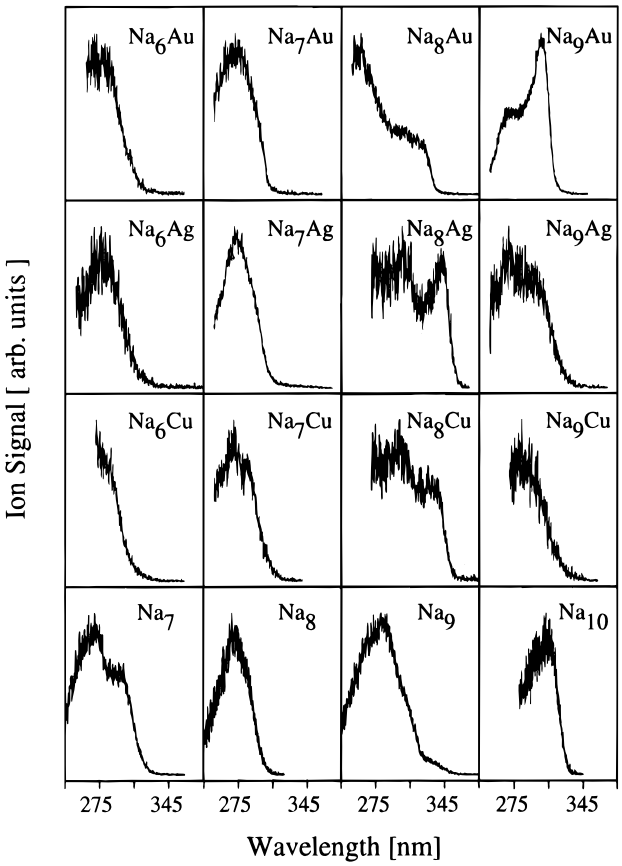

Figure 5. Intensity-normalized photoionization efficiency curves for Na_x, Na_xCu, Na_xAg, and Na_xAu clusters. Details concerning the measurements are given in the text. The extracted ionization potentials are summarized in Table 1.

structureless model. The pronounced cluster formation of the Na/Au system is explained with the use of molecular orbital arguments and the strong relativistic effects. For the coinage metals, differences in the relativistic effects are especially pronounced, as manifested, e.g., in the different colors of these metals. More specific information about the bonding in these different heteroclusters is obtained by using the quasiequilibrium theory to estimate free energies of selected elementary steps in the cluster formation process. In the second part of this section, the ionization potentials of the heteroclusters are tabulated and discussed.

But before we start with the main discussion, the influence of the expansion conditions on the neutral cluster distributions has to be addressed. For the comparison of the different heteroclusterings of sodium with copper, silver, and gold, the heteroclusters were generated at identical partial pressures. The resulting heterocluster distributions are used to get information about the binary alloying (Figures 2, 3a, and 4a). But using the same partial pressures for all coexpansions, the thermal formation histories are necessarily unique for each heterosystem, as the nozzle temperatures for the three expansions differ. This may, in turn, lead to different internal temperatures, resulting in kinetically controlled expansions for colder clusters and thermodynamically controlled expansions for hotter clusters. Such effects were studied extensively for the system Na/Ag. The results showed that kinetically controlled expansions show exponential cluster size distributions and thermodynamically controlled expansions sharp multimodal cluster size distributions. It turned out that at the above-mentioned conditions, the expansions for Na/Cu and Na/Ag are not yet fully thermodynamically controlled. This can be seen by the rather broad cluster distributions of the disilver heteroclusters (Figure 3a)

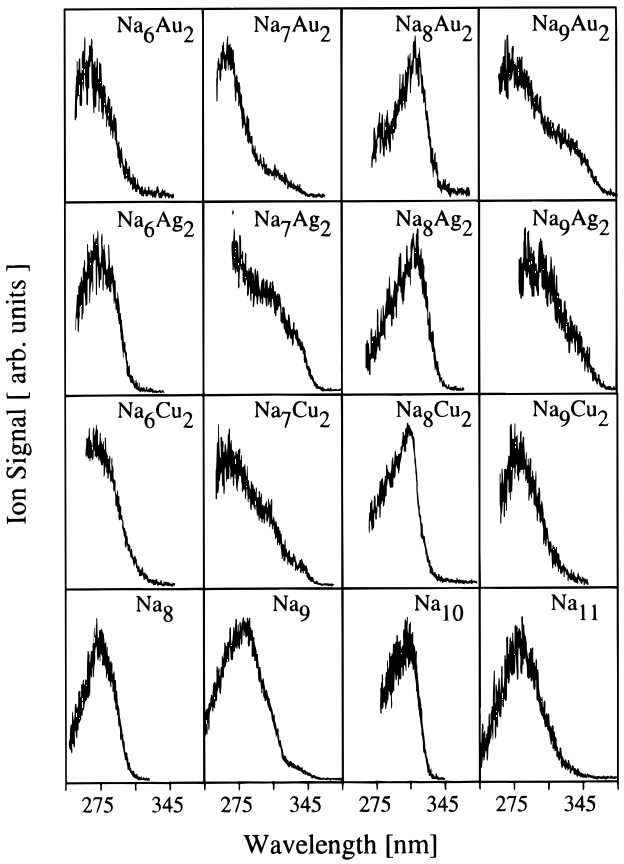

Figure 6. Intensity-normalized photoionization efficiency curves for Na_x, Na_xCu_2, Na_xAg_2, and Na_xAu_2 clusters. Details concerning the measurements are given in the text. The extracted ionization potentials are summarized in Table 1.

TABLE 1: Pseudo-Watanabe Ionization Potentials for Na_x and Na_xY (Y = Cu, Cu_2, Ag, Ag_2, Au, Au_2 Heteroclusters, with Errors in Parentheses)

x	Na_{x+1}	Na_xCu	Na_xAg	Na_xAu
3	4.24(02)		4.59(02)	
4	3.99(03)		4.16(03)	
5	4.23(03)	4.00(03)	4.29(03)	
6	4.03(03)	4.05(03)	3.98(04)	4.01(02)
7	4.22(03)	4.12(03)	4.13(02)	4.13(02)
8	3.56(05)	3.61(02)	3.52(02)	3.75(02)
9	3.84(03)	3.91(04)	3.84(05)	3.97(01)
x	Na_{x+2}	Na_xCu_2	Na_xAg_2	Na_xAu_2
4	4.23(03)		4.14(03)	
5	4.03(03)		3.99(03)	
6	4.22(03)	3.99(03)	4.12(03)	4.10(05)
7	3.56(05)	3.62(04)	3.56(03)	3.72(04)
8	3.84(03)	3.79(03)	3.77(03)	3.80(04)
9	4.04(04)	3.91(04)	3.49(05)	3.44(03)
x	Na_{x+3}	Na_xCu_3	Na_xAg_3	Na_xAu_3
5	4.22(03)		4.12(03)	
6	3.56(05)		3.55(04)	3.66(04)
7	3.84(03)		3.78(05)	
8	4.04(04)		3.55(04)	3.77(03)
9	3.85(03)		3.58(04)	

and of the mono- and dicopper heteroclusters (Figure 4a). In order to compare the cluster size distributions and relative cluster stabilities of the three heterosystems and to test the validity of the jellium model, we therefore carried out additional experiments for these two systems at higher oven temperatures. The resulting neutral cluster distributions show sharp shell closings (Figures 2, 3b, and 4b) and are therefore used for the purposes stated above.

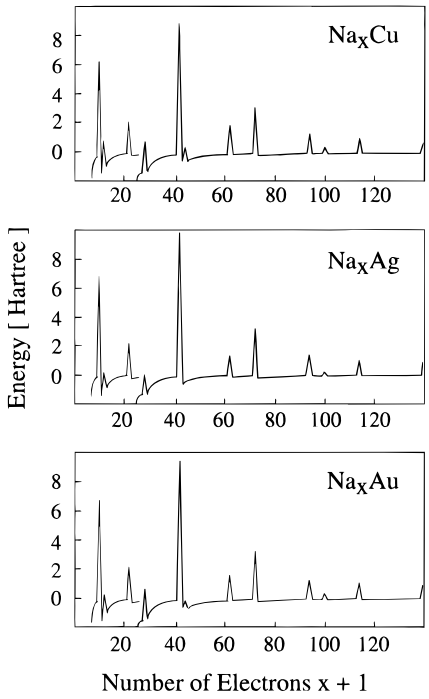

Figure 7. Second differences of total electronic energies (Δ^2E) as a function of the total number of valence electrons. These energy differences were calculated within the modified jellium model. Note that all three systems show the first three shell closings at 8, 10, and 20 valence electrons.

4.1. Metal Cluster Abundance Spectroscopy. *4.1.1. Relative Stabilities.* The observation of multimodal cluster distributions of sodium and their interpretation is cluster history.[23−25] Mass spectroscopic results on the coinage metals copper, silver, and gold are in accord with the shell structure observed for pure sodium clusters.[26] Furthermore, in photoelectron spectra of the coinage metal ions, the electron affinities and the onset of the d band have been studied as a function of the cluster ion size, showing that the trends of electron affinities are consistent with an ellipsoidal shell model.[27,28] Recent quantum chemical calculations showed that the s−d hybridization in these cluster is important but that the upper states are mostly s-like; therefore, pure coinage metal clusters reveal jellium features.[29,30]

Multimodal distributions for heteroclusters were first observed for K/Mg and K/Zn heteroclusters.[12,31] Among other interpretations, several approaches, including a structureless spherical jellium model with a modified Wood−Saxon potential, were used to explain the enhanced stability of the 10-electron systems (K_8Mg and K_8Zn). With the assumption that the heteroatom occupies the center of the cluster,[13,32] its higher ionization potential causes a central dip in the jellium potential well.[33] This stabilizes the electronic states with low angular momentum and consequently may lead to a 1d/2s level inversion for these two systems.[33] The same effects were observed for the Na/Zn,Cd,Hg[10] and Na/Ba,Eu,Sr,Ca,Yb,Mg[34] systems. Copper, silver, and gold also having higher ionization potentials than sodium reveal the same level inversion. The corresponding results of our calculations are shown in Figure 7. All three systems show the "Aufbau" principle, $(1s)^2(1p)^6(2s)^2(1d)^{10}(2p)^6(1f)^{14}$..., with the corresponding spherical shell closings for 2,8,10,20,26,40,..., valence electron systems and the 1s, 1p, 2s, 1d, ..., levels.

In the measured mass range, the Na/Cu and Na/Ag systems show agreement with this Aufbau principle, in which the eight valence electron clusters (Na_7Cu, Na_6Cu_2, Na_7Ag, Na_6Ag_2) are more stable than the decamers. The 2s/1d level inversion,

leading to the 20-electron closed-shell systems, is confirmed by the pronounced intensities of $Na_{19}Ag$, $Na_{18}Ag_2$, and $Na_{17}Ag_3$. The Na/Au system behaves differently. The first shell closing at the decamer reveals this 2s/1d inversion. The next stability maximum was found for the 18 valence electron system ($Na_{16}Au_2$). Within the jellium model, this can only be interpreted if there is no such inversion. For even bigger heteroclusters with three, four, and five heteroatoms, the mass spectral intensity maxima cannot be interpreted by the jellium model.

Mass spectral abundances suggest that the jellium behavior is most pronounced for the Na/Ag system. This is also supported by the largest drop of the ionization potentials for mixed Na/Ag clusters going from the octamer to the nonamer (Table 1). In fact, Na_xAg_y clusters are more weakly bonded (see below) than the corresponding Na_xAu_y clusters; this should be reflected in a smoother average intramolecular potential and, therefore, in a better condition for the validity of the jellium model. Furthermore, the electronegativity difference is lower in mixed sodium silver clusters than in mixed sodium gold clusters. Using the Pauling scale, they are 1.0 for sodium and silver and 1.5 for sodium and gold. This suggests a lower polarization, which means less directionalities of the metal metal bonds and, therefore, a better fulfillment of the jellium requirements. The reduced shell effect observed for Na_xAu_y can be explained reasonably by invoking the higher electronegativity differences and the d-electron participation in gold, which lead to a slightly more directional bond and therefore to a deterioration of the jellium model. This deterioration of the jellium model caused by more directionality in the bond is well-known, for example, in Al and Pb clusters.[35,36]

4.1.2. Binary Alloying of Clusters. A comparison of the three heterosystems shows the most pronounced heteroclustering for Na/Au coexpansions. This can be explained by the increased tendency of gold to form multiple d bonds, since the $^2S \Rightarrow {}^2D$ excitation energy in Au is smaller (1.13 eV) compared to 1.38 eV in Cu and 3.74 eV in Ag.[37] In addition, within group 11, the ratio of the orbital radii $\langle r_{(n+1)s}\rangle/\langle r_{nd}\rangle$ decreases with increasing mass. This is due to the relativistic contraction of the 6*s* orbital of gold together with the expansion of the 5*d* orbitals.[38] This in turn makes the d orbitals more accessible for bonding with ligand atoms and leads to a better overlap with the 3*s* orbitals of the neighboring sodium atoms in the cluster. This results in more stable heteroclusters but also in more directional bonds. In the gold dimer, these effects shorten the bond length by 0.3 Å, strengthen the bond by 0.38 eV,[39] and increase the vibrational frequency by 50%.[38]

These observed differences of the chemistry of the coinage metals reacting with sodium suggest that there are subtle differences in the metal−metal binding energies of the heteroclusters. But how can one obtain information about binding energies from molecular beam experiments? These differences in the binding energies should be visible in the free energies of substitution reactions where one sodium atom is replaced by a heteroatom. In an earlier work,[40] it was shown that quasiequilibrium theory can be applied to molecular beam experiments in order to calculate free-energy changes for reactions such as

$$Na_{n-x}Y_x + Y \Rightarrow Na_{n-(x+1)}Y_{x+1} + Na \quad (Y = Cu, Ag, Au)$$

The starting point of this ansatz is the observation of binomial mixed cluster distributions, where the relative ion abundances for a specific $Y_xNa_{n-x}^+$ (Y = Cu, Ag, Au) among an *n* atomic series are given by

TABLE 2: Free Enthalpies (ΔG) for the Substitution Reaction of Na_8Y (Y = Cu, Ag, Au) Clusters[a]

M	T_2, K	p°_M, Torr	α	γ	ΔG, eV (700/820 K)
Cu	1650	0.05	0.18	1633	−0.45/0.52
Ag	1400	0.05	0.11	998	−0.42/0.49
Au	1800	0.05	0.23	2087	−0.46/0.54

[a] The temperature T_1 of the large cartridge was 1100 K ($p_{Na} = 453.54$ Torr). The mole fraction α of the heterometals Cu, Ag, and Au was obtained from the binomial distribution analyses of the corresponding mass spectra. The agreement between measurements and binomial distribution determined in this way is generally good. The most common observed deviations are for pure sodium clusters which are underrepresented in the actual measurements. For the internal temperatures of the cluster, the limits of 700 and 820 K were measured.

$$I^+Y_xNa_{n-x} \propto \frac{n!}{x!(n-x)}\alpha_x(1-\alpha)^{n-x} \tag{1}$$

The probability α corresponds to the mole fraction of the heteroatom Y in the cluster and is calculated as

$$\alpha(n) = \frac{\sum_{x=0}^{n} x\,I[Na_{n-x}Y_x]}{n\sum_{x=0}^{n} I[Na_{n-x}Y_x]} \tag{2}$$

Let us assume that the value of α is equal to the mole fraction of the heteroatom Y during the cluster formation process, determined by the corresponding vapor pressures in the two oven chambers. In this case, the observation of a binomial distribution means that the cluster formation process which involves multiple sequential aggregation/collisional and (or) evaporative cooling cycles[41,42] is purely statistical. This is only possible if there are no differences in binding energies in the heteroclusters. In the case where α is larger than the initial mole fraction of the heteroatom Y, the cluster formation process favors the incorporation of an atom Y into the heterocluster. The degree of this enhancement γ, which is calculated by eq 3 with p°_x as the partial pressures of the two metals in the coexpansion, is a function of the system thermodynamics (eq 4):

$$y(n) = \frac{\alpha(n)}{\dfrac{p^\circ_B}{P^\circ_A + p^\circ_B}} \tag{3}$$

$$\Delta G = -RT\ln(\gamma) \tag{4}$$

If the internal temperatures of the clusters are known, free-energy changes can be estimated for different elementary steps in the clustering process.

Enrichment factors γ for the three heterosystems and free energies ΔG for reactions I, II, and III are summarized in Table 2. The internal temperatures which are used for the calculation

$$Na_8Cu + Cu \Rightarrow Na_7Cu_2 + Na \text{ (I)}$$

$$Na_8Ag + Ag \Rightarrow Na_7Ag_2 + Na \text{ (II)}$$

$$Na_8Au + Au \Rightarrow Na_7Au_2 + Na \text{ (III)}$$

of the free-energy changes of these representative reactions were estimated from the thermal tail of the corresponding PIE curves[43] and assuming an evaporative cooling of 400 K.[44] For Na_8Ag

and Na_7Ag_2, internal temperatures of about 300 and 420 K, respectively, were obtained. After adding the evaporative cooling, they are used as lower and upper temperature limits.

From this analysis, the following conclusions can be made:

1. The differences in the binding energies of the heterodimers CuNa,[45] AgNa,[46] and AuNa[47] and homodimers Cu_2, Ag_2, and Au_2[48] (−0.21, −0.26, and −0.14 eV, respectively) are smaller than the measured free energies of reactions I−III. The relative values are significantly different. In the dimer case, the substitution of a sodium atom by a silver atom is thermodynamically most favored. In the nine-atom clusters, it is just the opposite. Assuming that the two heteroatoms are adjacent in the cluster, the most significant difference between the two cases is the presence of a solvation of the dimer in the cluster case. We thus may argue that the observed deviations of the free energies are due to a different interaction of the three dimers with the sodium ligand sphere. This indicates that the interaction of Ag_2 with the sodium ligand sphere is the weakest. In fact, a similar trend was observed for the reactivity of the three coinage metal dimers with ammonia where the binding energy of ammonia with Ag_2 (14 kcal/mol^{-1}) is smaller by a factor of 2 than it is for Cu_2 (>25 kcal/mol^{-1}) and Au_2 (>30 kcal/mol^{-1}).[49] These differences are interpreted as the consequence of the enhanced destabilization of the *d* electrons in gold, which results in a stronger interaction with the ligands.[50]

2. The reciprocal ratio of the $^2S \Rightarrow {}^2D$ excitation energy for Cu (1.38 eV):Ag (3.74 eV):Au (1.13 eV) = 1:0.38:1.22 shows the same trend as the ratio of the enrichment factors γ(Cu):γ(Ag):γ(Au) = 1:0.61:1.28. This is another indication that the stability of the heteroclusters is partly controlled by the ease of the s−d hybridization and that the large enrichment of gold is due to the enhanced interaction of the d orbitals with the s orbitals of sodium.

3. The differences of the binding energies of bulk sodium with Cu, Ag, and Au (Cu−Na, 2.377 eV; Ag−Na, 1.837 eV; Au−Na, 2.697 eV) are 4−5 times larger than the measured ΔG values for the three reactions. This is not surprising since the band structure is not yet developed in such small entities.

4.2. Ionization Potentials. Table 1 shows the pseudo-Watanabe IP values[22] extracted from the PIE curves of the different heteroclusters. This table is incomplete since certain clusters could not be detected or the intensity was too low to perform accurate measurements. Besides the well-known odd−even effect,[25] a distinct drop of the vertical ionization potential is observed in all cases going from the eight-valence-electron cluster to the nonamer. This is consistent with the second shell closing predicted by jellium calculations. For the disilver and digold heteroclusters, the $(1s)^2(1p)^6(2s)^2$ shell closing is moderately present. This jellium behavior of the ionization potentials was also observed by Kaya et al. for larger Na/Au heteroclusters. The IP's of the Au_nNa_m clusters ($n = 6-13$; $m = 0-10$) were measured using a doubled dye laser.[51] In this work, a discontinuous drop of the IP was observed when one sodium atom was added to the $Au_{11}Na_7$, $Au_{12}Na_6$, $Au_{13}Na_5$, and $Au_{13}Na_7$ clusters.

It is interesting to observe that this drop in IP is most pronounced for the Na/Ag system. With IP drops in the range of 0.56 and 0.61 eV at the second shell closing, this heterosystem behaves similarly to pure sodium clusters which have a corresponding drop of 0.66 eV. The weakest drops (0.36−0.38 eV) are observed for the Na/Au system.

A comparison with the observed shell closings in the cluster abundances indicates that in the cases of Na_7Ag, Na_6Ag_2, Na_5Ag_3, Na_7Cu, and Na_6Cu_2, thermodynamic and electronic stabilities coincide. If we turn our attention to the far most stable cluster Na_8Au_2, then the relative weak drop of the IP at the decamer suggests that its enhanced thermodynamic stability is not purely due to an electronic stabilization. Due to the largest difference in electronegativities of sodium and gold, the charge transfer may lead to a slight structure-dependent Coulomb contribution to its stability.

5. Conclusions

In a first approach, one expects a similar cluster formation of copper, silver, and gold with sodium due to their common $^2S_{1/2}$ ground state. In this work, quite a different heteroclustering was observed for the three systems. The heterocluster formation for the Na/Au system is the most pronounced, showing heteroclusters with up to five heteroatoms. For the Na/Cu system, the measured heterocluster intensities are smaller by a factor of 20, and only heteroclusters with one or two copper atoms are observed. The pronounced heterocluster formation of gold and sodium can be explained by the availability of gold 5d orbitals for the metal−metal interaction due to the relativistic contraction of the 6s orbitals of gold and the smallest $^2S \Rightarrow {}^2D$ excitation energy. This trend of an enhanced interaction of gold with sodium is also reflected in the phase diagrams of the solids of these alloys. These show three different phases with the compositions of NaAu, Na_2Au, and $NaAu_2$ for the Na/Au system, one intermetallic phase with the stoichiometric composition of $NaAg_2$ for the Na/Ag system, and no miscibility for the Na/Cu system.[52]

For Na/Au expansions, distinct cluster intensity maxima are observed for monoheteroclusters with 10 (Na_9Au) and 20 ($Na_{19}Au$) atoms. Diheteroclusters reveal enhanced stabilities for the 10 (Na_8Au_2) and 18 ($Na_{16}Au_2$) atom clusters. Tri-, tetra-, and pentagold heteroclusters reveal no cluster distributions which can be explained by the jellium model. In contrast, neutral cluster distributions of the heterosystem Na/Ag show closed shells for the 8 (Na_7Ag, Na_6Ag_2, Na_5Ag_3) and 20 ($Na_{19}Ag$, $Na_{18}Ag_2$, $Na_{17}Ag_3$) atom clusters in the entire measured mass range. For the Na/Cu system, closed shells at the eight-atom clusters (Na_7Cu, Na_6Cu_2) are observed.

For all three systems, a distinct drop of the ionization potentials was measured between the octamer and the nonamer. This drop is most marked for the Na/Ag system (up to 0.61 eV), whereas it is only around 0.37 eV for the Na/Au system. The Na/Ag system shows the most pronounced similarities to pure sodium clusters regarding relative cluster stabilities and the drop of the ionization potential at the second shell closing.

Differences in free energies (ΔG) of the exchange of a heteroatom with sodium for the species Na_8X (X = Cu, Ag, Au) assuming a cluster temperature of 700 K are −0.45, −0.42, and −0.46 eV for gold, silver, and copper, respectively. Relative differences in dimer values are interpreted as differences in the sodium solvation of the heterodimers. It is suggested that this solvation energy is smallest for Ag_2.

Acknowledgment. This research was performed at the University of Bern with the support of the Swiss National Science Foundation (Grant 2.348−0.86.). We thank Dr. H. M. Frey, Dr. U. Roethlisberger, and Dr. C. Yeretzian for their support and N. Roesch and M. Stener for helpful discussions.

References and Notes

(1) Pettifor, D. G. *The Science of New Materials*; Briggs, A., Ed.; Wolfson College Lecture; Blackwell: Oxford, 1992; p 86 and references therein.

(2) Kienast, G.; Verma, J. *Z. Anorg. Chem.* **1961**, *310*, 143.

(3) Koenig, C.; Christensen, N. E.; Kollar, J. *Phys. Rev. B* **1984**, *29*, 6481.

(4) Spicer, W. E. *Phys. Rev.* **1962**, *125*, 1297.

(5) Ashcroft, N. W.; Mermin, N. D. *Solid State Physics*; Saunders College: Philadelphia, PA, 1976.

(6) Kittel, Ch. *Festkoerperphysik*; R. Oldenbourg Verlag: Muenchen, Wien, 1988.

(7) Kopitzki, K. *Einfuehrung in die Festkoerperphysik*; Teubner Studienbuecher Physik: Stuttgart, 1989.

(8) Rodriguez, J. A.; Goodman, D. W. *Science* **1992**, *257*, 897 and references therein.

(9) Campbell, C. T. *Annu. Rev. Chem.* **1990**, *41*, 775.

(10) Heiz, U.; Röthlisberger, U.; Vayloyan, A.; Schumacher, E. *Isr. J. Chem.* **1990**, *30*, 147.

(11) Kappes, M. M.; Radi, P.; Schaer, M.; Yeretzian, C.; Schumacher, E. *Z. Phys. D—Atoms, Molec. Clusters* **1986**, *3*, 115.

(12) Bréchignac, C.; Cahuzac, P. *Z. Phys. D.—Atoms, Molec. Clusters* **1986**, *3*, 121.

(13) Heiz, U.; Vayloyan, A.; Schumacher, E.; Yeretzian, C.; Stener, M.; Roesch, N. *J. Chem. Phys.*, in press.

(14) Nakajima, A.; Hoshino, K.; Naganuma, T.; Sone, Y.; Kaya, K. *J. Chem. Phys.* **1991**, *95*, 7061.

(15) Nakajima, A.; Kishi, T.; Kaya K. *Chem. Phys. Lett.* **1991**, *187*, 239.

(16) Hoshino, K.; Naganuma, T.; Watanabe, K.; Nakajima, A.; Kaya, K. *Chem. Phys. Lett.* **1993**, *211*, 571.

(17) Nakajima, A.; Hoshino, K.; Sugioka, T.; Naganuma, T.; Taguwa, T.; Yamada, Y.; Watanabe, K.; Kaya, K. *J. Phys. Chem.* **1993**, *97*, 86.

(18) Kappes, M. M.; Schär, M.; Schumacher, E. *J. Phys. Chem.* **1987**, *91*, 658. Kappes, M. M.; Schär, M.; Radi, P.; Schumacher, E. *J. Chem. Phys.* **1986**, *841*, 863.

(19) Inghram, M.; Hayden, R. *N.A.S.N.R.C* Publ. 311. Kappes, M. M.; Leutwyler, S. *Atomic and Molecular Beams Methods*; Scoles, G., Ed.; Oxford University: Oxford, 1988; Vol. 1.

(20) Kappes, M. M.; Schaer, M.; Schumacher, E.; Vayloyan, A. *Z. Phys. D* **1987**, *5*, 359.

(21) (a) Bréchignac, C.; Cahuzac, Ph.; Roux, J. *J. Chem. Phys.* **1987**, *87*, 229. (b) Bréchignac, C.; Cahuzac, Ph.; Roux, J.; Pavolini, D.; Spiegelmann, F. *J. Chem. Phys.* **1987**, *87*, 5694. (c) Bréchignac, C.; Cahuzac, Ph.; Leygnier, J.; Weiner, J. *J. Chem. Phys.* **1989**, *90*, 1492.

(22) Kappes, M. M.; Schaer, M.; Roethlisberger, U.; Yeretzian, C.; Schumacher, E. *Chem. Phys. Lett.* **1988**, *143*, 251.

(23) (a) Herrmann, A.; Leutwyler, S.; Schumacher, E.; Wöste, L. *Helv. Chim. Acta* **1978**, *614*, 53. (b) Kappes, M. M.; Kunz, R. W.; Schumacher, E. *Chem. Phys. Lett.* **1982**, *91*, 413.

(24) Knight, W. D.; Clemenger, K.; de Heer, W. A.; Saunders, W. A.; Chou, M. Y.; Cohen, M. L. *Phys. Rev. Lett.* **1984**, *52*, 2141.

(25) de Heer, W. A. *Rev. Mod. Phys.* **1993**, *65*, 611.

(26) Katakuse, I.; Ichihara, T.; Fujita, Y.; Matsuo, T.; Sakurai, T.; Matsuada, H. *Int. J. Mass Spect. Ion Proc.* **1985**, *67*, 229.

(27) (a) Cheshnovsky, O.; Taylor, K. J.; Conceicao, J.; Smalley, R. E. *Phys. Rev. Lett.* **1990**, *64*, 1785. (b) Taylor, K. J.; Pettiette-Hall, C. L.; Cheshnovsky, O.; Smalley, R. E. *J. Chem. Phys.* **1992**, *4*, 3319.

(28) (a) Cha, C.-Y.; Ganteför, G.; Eberhardt, W. *J. Chem. Phys.* **1993**, *99*, 6308. (b) Handschuh, H.; Cha, C.-Y.; Möller, H.; Bechthold, P. S.; Ganteför, G.; Eberhardt, W. *Chem. Phys. Lett.* **1994**, *227*, 496.

(29) Bonacic-Koutecky, V.; Cespiva, L.; Fantucci, P.; Koutecky, J. *J. Chem. Phys.* **1993**, *987*, 981.

(30) Massobrio, C.; Pasquarello, A.; Car, R. *Chem. Phys. Lett.* **1995**, *238*, 215.

(31) Kappes, M. M.; Radi, P.; Schaer, M.; Schumacher, E. *Chem. Phys. Lett.* **1985**, *119*, 11.

(32) Bonacic-Koutecky, V.; Cespiva, L.; Fantucci, P.; Fuchs, C.; Guest, M. F.; Koutecky, J.; Pittner, J. *Chem. Phys.* **1994**, *186*, 275.

(33) Schumacher, E.; Blatter, F.; Frey, M.; Heiz, U.; Roethlisberger, U.; Schaer, M.; Vayloyan, A.; Yeretzian, C. *Chimia* **1988**, *42*, 357 and references therein.

(34) Yeretzian, C. *J. Phys. Chem.* **1995**, *99*, 123.

(35) Begemann, W.; Meiwes Broer, K.; Lutz, H. *Phys. Rev. Lett.* **1986**, *56*, 2248.

(36) Phillips, J. *Chem. Rev.* **1986**, *86*, 619.

(37) Moore, C. E. *Atomic Energy Levels, Nat. Bur. Stand. (US) Circ. 467, Vols. II and III*; U.S. GPO: Washington, D.C., 1952; p 1958.

(38) Lee, Y. S.; Ermler, W. C.; Pitzer, K. S. *J. Chem. Phys.* **1979**, *70*, 288.

(39) Schwerdtfeger, P.; Dolg, M.; Schwarz, W. H.; Bowmaker, G. A.; Boyd, P. D. W. *J. Chem. Phys.* **1991**, *91*, 1762.

(40) Kappes, M. M.; Schaer, M.; Schumacher, E. *J. Phys. Chem.* **1987**, *91*, 658.

(41) (a) Klots, C. E. *Z. Phys. D—Atoms, Molec. Clusters* **1991**, *20*, 105. (b) Klots, C. E. *J. Chem. Phys.* **1985**, *83*, 5854. (c) Klots, C. E. *Nature* **1987**, *327*, 222.

(42) (a) Gspann, J. In *Physics of electronic and atomic collisions*; Datz, S., Ed.; North Holland: Amsterdam, 1982; pp 79−96. (b) Gspann, J. In *Metal clusters*; Träger, F., Putlitz, G., Eds.; Springer: Berlin, 1986; pp 43−45.

(43) Roethlisberger, U.; Schaer, M.; Schumacher, E. *Z. Phys. D—Atoms, Molec. Clusters* **1989**, *13*, 171.

(44) Hansen, K.; Falk, J. *Z. Phys. D* **1995**, *34*, 251.

(45) Piacente, V.; Gingerich, K. A. *Naturforsch. Teil A* **1973**, *28*, 316.

(46) Piacente, V.; Gingerich, K. A. *High Temp. Sci.* **1972**, *4*, 312.

(47) Busse, B.; Weil, K. G. *Ber. Buns. Phys. Chem.* **1981**, *85*, 309.

(48) Morse, M. D. *Chem. Rev.* **1986**, *86*, 1049.

(49) Hackett, P. A.; Mitchell, S. A.; Rayner D. M.; Simard, B. *Metal−Ligand Interactions: Structure and Reactivity*; Russo, N., Salahub D., Eds.; NATO ASI Series C: Mathematical and Physical Sciences XXX; Kluwer: Dordrecht, 1994.

(50) Lian, L.; Akhtar, F.; Hackett, P. A.; Rayner, D. M. *Chem. Phys. Lett.* **1993**, *205*, 487.

(51) Hoshino, K.; Naganuma, T.; Watanabe, K.; Nakajima, A.; Kaya, K. *Chem. Phys. Lett.* **1993**, *211*, 571.

(52) Kienast, G.; Verma, J. *Z. Anorg. Allg. Chem.* **1961**, *310*, 143.

JP9609388